

# Q1 Catadioptric panoramic stereovision for humanoid robots†

2 C. Salinas‡, H. Montes‡§\*, G. Fernandez¶, P. Gonzalez de Santos‡, Q2 and M. Armada‡

4 ‡Centre for Automation and Robotics – CAR (CSIC-UPM), Robotics Locomotion & Interaction Group, Ctra.  
5 de Campo Real. Km 0.200, La Poveda, Arganda del Rey, 28500, Madrid, Spain

6 §Facultad de Ingeniería Eléctrica, Universidad Tecnológica de Panamá, Republic of Panama

Q3 ¶Departamento de Electrónica y Circuitos, Simón Bolívar University, Republic of Venezuela

8 (Accepted August 25, 2011)

## 9 SUMMARY

10 This paper proposes a novel design of a reconfigurable  
11 humanoid robot head, based on biological likeness of  
12 human being so that the humanoid robot could agreeably  
13 interact with people in various everyday tasks. The proposed  
14 humanoid head has a modular and adaptive structural design  
15 and is equipped with three main components: frame, neck  
16 motion system and omnidirectional stereovision system  
17 modules. The omnidirectional stereovision system module  
18 being the last module, a motivating contribution with  
19 regard to other computer vision systems implemented in  
20 former humanoids, it opens new research possibilities for  
21 achieving human-like behaviour. A proposal for a real-  
22 time catadioptric stereovision system is presented, including  
23 stereo geometry for rectifying the system configuration and  
24 depth estimation. The methodology for an initial approach  
25 for visual servoing tasks is divided into two phases, first  
26 related to the robust detection of moving objects, their  
27 depth estimation and position calculation, and second the  
28 development of attention-based control strategies. Perception  
29 capabilities provided allow the extraction of 3D information  
30 from a wide range of visions from uncontrolled dynamic  
31 environments, and work results are illustrated through a  
32 number of experiments.

33 **KEYWORDS:** Catadioptric panoramic cameras; Omnidirec-  
34 tional stereovision; Visual servoing control; Humanoid robot  
35 head.

## 36 1. Introduction

37 During last years, several research groups have achieved  
38 important advances in humanoid robotics projects.<sup>1–2</sup> At its  
39 inception, research efforts were concentrated in the areas  
40 of design and construction of biped robots. However, over  
41 the years greater emphasis has been given to technological  
42 and scientific development, which aims at achieving a higher

affinity interaction with human beings, developing humanoid  
robots with friendly aspects.

The development of humanoid robots that assist human  
activities in environments such as offices, homes, shops and  
hospitals is expected. Humanoid robots are called upon to  
perform these tasks for serving humans because of their  
anthropomorphic structure, friendly design, locomotion way  
and so forth. Human society demands the incorporation  
of new applications for robots to perform various tasks  
of service, assistance, entertainment<sup>3</sup> and so on. In these  
tasks, robots will be required to interact with the modifiable  
environment and surrounded by people.

Most works on humanoid robots, up to date, have  
concentrated on studying the locomotion problem. In this  
direction great advances have been achieved and humanoid  
robots like ASIMO, HRP-2, the QRIO, Johnnie,<sup>1–4</sup> among  
others, can be mentioned.

The vision system (based on conventional cameras)  
on these robots in combination with other sensors and  
appropriate control strategies are used to improve the process  
of robot movement.<sup>8–11</sup>

By other side, during last two decades interest in panoramic  
vision systems has grown and their use in the robotics field  
has gained importance due to technological advances and  
the increasing need to track and detect objects over large  
3D environments. However, the incorporation of panoramic  
vision into the field of humanoid robots is not yet broadly  
used. In the case of omnidirectional vision systems, since  
the Ress' first proposal in US Patent No. 3505465 in 1970<sup>12</sup>  
and later on when these systems started to develop again,<sup>13–15</sup>  
several configurations and theories of catadioptric panoramic  
system have been presented in order to obtain images of the  
entire scene.<sup>16–18</sup>

Compared with conventional systems, their greatest  
advantage is to acquire a wide range of view images, which  
allow robotic systems to become more suitable for tasks such  
as navigation, tracking objects and ego-motion detection,  
since the objects disappear later on the images.

It is common to use rotating, multiple cameras, or  
catadioptric systems to obtain images of the entire scene.  
However, the first approach brings in mechanical problems,  
as the movement of heavy parts, the manufacture costs and  
the rotation mechanisms are not always suitable for real-  
time applications, and also to achieve accurate positioning

Q4 \* Corresponding author. E-mail: hector.montes@csic.es

† This paper was originally submitted under the auspices of the  
CLAWAR Association. It is an extension of work presented at  
CLAWAR 2009: The 12th International Conference on Climbing  
and Walking Robots and the Support Technologies for Mobile  
Machines, Istanbul, Turkey.

43  
44  
45  
46  
47  
48  
49  
50  
51  
52  
53  
54  
55  
56  
57  
58  
59  
60  
61  
62  
63  
64  
65  
66  
67  
68  
69  
70  
Q5 71  
72  
73  
74  
75  
76  
77  
78  
79  
80  
81  
82  
83  
84  
85  
86

it requires extra efforts. Multiple cameras present a high computing cost to form a single panoramic image. On the other hand, the catadioptric systems as the result of combination of a refracting (*dioptric*) and reflecting (*catoptrics*) surfaces are considered to be a very interesting configuration. These systems are easily built employing a conventional high-resolution camera as the refracting part and a curved mirror as the reflecting one. In order to acquire a single image containing the information of the whole scene, the camera and mirror must be arranged in a configuration such that the entire system has a *single effective viewpoint*,<sup>18</sup> named as *central catadioptric cameras*.<sup>19</sup> To generate omnidirectional images perfect quadric surfaces are considered as the only candidates for mirror shapes; in this way every incident ray of light that strikes the surface towards the mirror focus is reflected to the second focus. Since the geometry of the system is known, it is possible to compute the ray direction for each pixel and its irradiance value.

Several configurations of stereo system have been presented: The general theory of epipolar geometry for central catadioptric stereo cameras is depicted in ref. [19], a rectified systems is given in ref. [20], where two omnidirectional systems were placed one on top of the other, vertically aligned, the special mirror as a double lobbed in ref. [21], and a series of pairs of distinct curved mirrors with a single camera were proposed by Nene and Nayar.<sup>22</sup> Since our interest lies in high resolution systems, the last two configurations are to be avoided. A rectified system is desirable as it allows simplifying the process of disparity extraction, since the epipolar lines correspond to the radial axis of the omnidirectional image, even though the dimensions of this system for humanoid robot head are too large and not proportioned for a normal size human head.

The Robotics Locomotion and Interaction Group of the Centre for Automation and Robotics of the CSIC-UPM has been conducting research in the field of humanoid robotics. Currently this centre has a humanoid robot prototype called SILO2.<sup>23,24</sup> Also, this group has proposed an initial design of a multi-sensor humanoid head with omnidirectional vision system.<sup>25</sup>

This paper presents the extension and improvement of the first design of the humanoid head. In this extension, the work has been focused on a modular, flexible and adaptable design of the structure of the humanoid head, with which it is possible to experiment a range of actions and mechanisms of motion for the neck, and with various omnidirectional vision systems. Single omnidirectional or omnidirectional stereovision systems can be used, without these changes affecting the harmony of head design. The omnidirectional vision system will provide an extra sense to the robotic system, and at the same time it can bring in a substantial difference with relation to other humanoid robots that presently exist. The omnidirectional stereovision system presented in this work consists of two catadioptric panoramic systems aligned and separated by a constant horizontal distance, and displaced along the vertical axis at a preset distance.

The control system to develop the proposed strategies in this approach has a hierarchical architecture. The hardware consists of an industrial PC Intel Core 2 Duo based processor

E4500, 2.2 GHz for the omnidirectional vision system with Windows XP OS, and a Master/Server single board computer Pentium III, 700 MHz+, with QNX 6.4 RTOS, for controlling the installed servomotors in the neck of the humanoid head by means of three PID/slave processors. In addition, the system has a server–client architecture for servoing commands between both PCs.

This paper is divided into six sections. Section 1 introduces the topic of humanoid robotics and the motivation of this work, taking into account the humanoid head design, vision systems in humanoid robots and a brief review of omnidirectional vision systems. In Section 2 design features of the humanoid head are presented. Next, in Section 3 the description of a designed omnidirectional catadioptric system as well as a brief review of hyperbolic surface geometry, the system resolution and the corresponding panoramic transformation of our homemade specially designed mirrors is carried out. Our proposal for a real-time catadioptric stereovision system is presented in Section 4, including stereo geometry for rectifying the system configuration and depth estimation. The experimental stage focused to achieve human-like behaviours (humanoid head attitudes) is divided into two phases, first phase being the depth estimation and position calculation of the moving objects, and the second one being the development of attention-based control strategies. Finally, in last section conclusions and contributions of this work are presented.

## 2. Design of Humanoid Head

In the design of a humanoid head several aspects must be considered, the anthropometrical aspects being the most important ones, which refer to the study of physical dimensions of human body, and ensure that the humanoid head has similar proportions to its biological simile. Therefore, it is necessary to evaluate the parameters of human dimensions to achieve a humanoid-appropriate configuration.<sup>26</sup> It must also be taking into consideration the characteristics of human movement, in this case the neck movements. It is also important that the structural design of the humanoid head has the ability for sensors and actuators to be carried inside.

Moreover, it is necessary to consider issues related to the sensory system, in this case an omnidirectional stereovision system, allowing the acquisition of a wide range of views of approximate 360°.<sup>14,15</sup>

For the humanoid head of this work, the chosen vision system is formed by catadioptric systems. These vision systems can acquire a range of visions of  $\sim 360^\circ$  with the capture of a single image. Since the geometry of the mirror is known, the rectification of the omnidirectional image to panoramic one is possible.

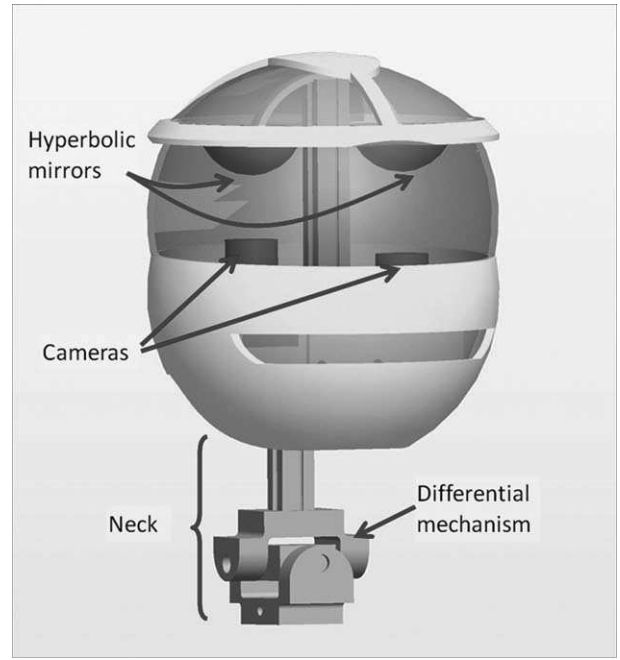
On the other hand, the dimensions of the system could be modified by means of adjustment of the mathematical model of the mirror surface if the profile of the mirror is changed.

### 2.1. Anthropometric and kinematic considerations

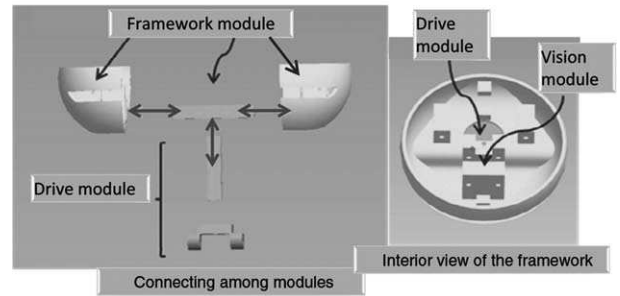
For the integration of robots in human society, it is essential to know the shapes and symmetries of human beings (as far as possible). So, humanoid robots must be designed with

Table I. Range of movement of the human neck.

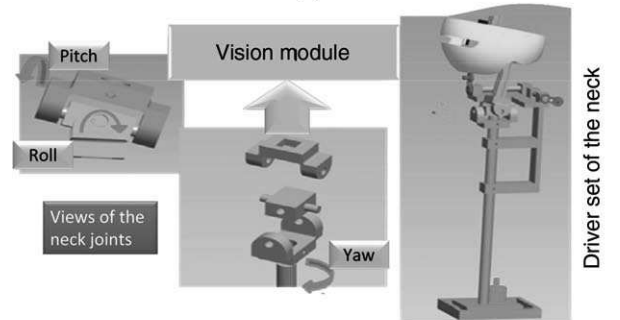
Vertebrae	Pitch (°)	Yaw (°)	Roll (°)
Upper cervical (C1–C2)	40	77	13
Lower cervical (C2–C7)	82	55	67
Total range	122	132	80



(a)



(b)



(c)

Fig. 1. (Colour online) (a) View of the humanoid head; (b) connection points among the three modules of the humanoid head; (c) motion module of the neck.

204 dimensions and characteristics similar to humans. These  
 205 concepts make it easy for humans “to accept” the humanoid  
 206 robots in their environment, e.g. offices, homes, shops,  
 207 exhibition spaces, hospitals. Montes *et al.*<sup>25</sup> describe the most  
 208 important parts of human skull used as a biological simile for  
 209 the design of the structure of the proposed humanoid head.

210 Similarly, it is required that both the positions and the  
 211 transitions between movements of robotic devices are as  
 212 soft and natural as possible. The study of neck movements  
 213 have enabled the realisation of the design of mechanisms to  
 214 execute movements similar to those of human beings.

215 In the case of human body, the head movement is achieved  
 216 by the combination of cervical vertebrae and neck muscles.  
 217 The human neck has three degrees of freedom, which are  
 218 presented in the movement of pitch, roll and yaw. Table I  
 219 details the range of neck motion.<sup>27</sup>

220 **2.2. Description of humanoid head**

221 The projected humanoid head is designed as a flexible and  
 222 adaptable system that consists of three modules. The first  
 223 module, the frame, is structural and it has the shape of  
 224 human head. The second module corresponds to the neck  
 225 motion system (motive module), consisting of mechanical  
 226 elements and electrical actuators. The actuators are three  
 227 DC motors with incremental encoders and gearboxes; two  
 228 of them are assembled around a differential gear to perform  
 229 pitch and roll movements, and the other actuator supports  
 230 the humanoid head and it performs the yaw movement.  
 231 Omnidirectional vision system is located in the third module,  
 232 which can be reconfigured to “single-omnidirectional” or  
 233 “stereo-omnidirectional” system. Figure 1(a) shows the  
 234 perspective view of the humanoid head design and its main  
 235 parts. Figure 1(b) shows the connecting points between  
 236 different modules. It is possible to see in Fig. 1(b) that each  
 237 module can operate independently and can be replaced by  
 238 other mechanisms (in the case of neck). These changes would  
 239 not affect the modules of frame and vision.

240 The external module or frame consists of three parts, two  
 241 of them form the lower part of the humanoid head and  
 242 correspond to the set comprising occipital, temporal and  
 243 maxilla, and the third part consists of the frontal–parietal  
 244 zone; both parts have been described by Montes *et al.*<sup>25</sup>

245 The module of the neck motion corresponds to the motion  
 246 module of the humanoid head. The pieces of this set are  
 247 joined to the bottom of the vision system module (see  
 248 Fig. 1(b)). This module includes a mechanism that allows  
 249 the performance of movements similar to those of human  
 250 movements (see Fig. 2). In addition, the flexibility of the  
 251 humanoid head design makes it possible to attach another  
 252 actuation mechanism.

253 Figure 1(c) shows the components of the motion module of  
 254 the neck. This module consists of a differential mechanism,

255 whose axes are connected to motors that carry out the  
 256 respective movements of pitch and roll. The yaw movement  
 257 is achieved through a vertical shaft attached to the top of the  
 258 differential mechanism. The motor of this shaft is installed  
 259 at the base of the neck of the head. The motors connected  
 260 to the differential mechanism are of same mechanical and  
 261 electric characteristics so that movements of pitch and  
 262 roll are carried out properly. These motors are 24 VDC, with  
 263 similar gearbox and differential encoders of 500 pulses

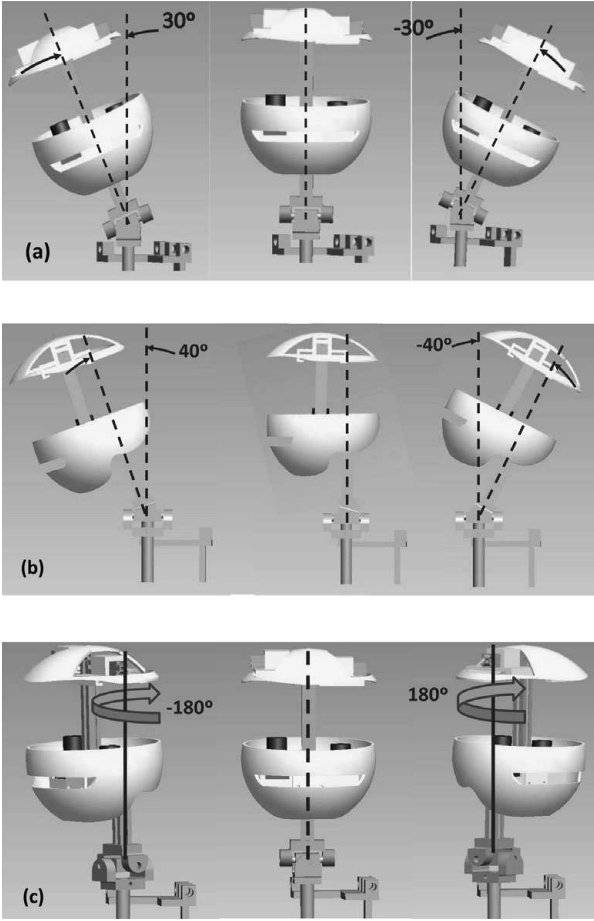


Fig. 2. Simulation of neck movement: (a) roll movement; (b) pitch movement and (c) yaw movement.

per revolution (using the appropriate hardware, it gets an accuracy of about  $0.0013^\circ$ ). The motor that performs the yaw movement has similar characteristics as the other two, but has less power and gearing because the gravitational effects are almost insignificant.

In this first prototype of the neck mechanism, the movements of pitch and roll have ranges of angular displacement lower than those of human beings (see Table I in Section 2.1). The range of angular displacement for the movement of pitch is  $-40^\circ \leq p1 \leq 40^\circ$  and for the movement of roll it is  $-30^\circ \leq r1 \leq 30^\circ$ , and the yaw movement is  $-90^\circ \leq y1 \leq 90^\circ$ . The first two movements are restricted by the mechanical system, and the control algorithm restricts the yaw movement. These movements have been outlined in Fig. 2.

The adaptive design of the humanoid head and neck structure that supports the head has been very useful for carrying out the experiments presented in this work. Since the design of the humanoid head presented in this paper has a modular architecture (as described above), it is possible to perform various experiments with different configurations of the omnidirectional vision. The shape and dimensions of the humanoid head can be changed without affecting the vision system. The interior structure of the head set allows the implementation of different vision systems (different hyperbolic mirrors, cameras, etc) without affecting the overall design of the head. Other adaptive characteristic of

the humanoid head is its capability for implementing diverse mechanisms of neck. The entire set of the head and vision system is supported by the mechanism of neck. This set can be coupled with any other possible mechanism used as neck.

### 3. Designing a Catadioptric Omnidirectional System

The catadioptric panoramic systems, also named as omnidirectional systems because of their enclosed information captured from a scene in all possible directions around an effective viewpoint, are based on a combination of conventional cameras and rotationally symmetric quadric mirrors, where the optical axis and the symmetric mirror axis are aligned. The theory of central perspective projections for a catadioptric image formation has been detailed in refs. [17, 18], where a collection of specific mirror shapes is analysed to achieve a single effective viewpoint that allows the construction of the perspective and panoramic images. Since the image formation is a well-controlled process, it is easy to derive its geometrical properties.

In order to present the geometry of image formation for central catadioptric cameras, the notation of points in the 3D space is chosen to be represented by bold upper case letter, such as  $\mathbf{X}$ , and its corresponding coordinates by italic upper case letter, such as  $X$ . For the representation of points in a 2D space, a bold lower case letter is used, and for its corresponding coordinates are represented by italic lower case letters. The same notation is used for 2D or 3D vectors and planes.

The vision systems designed in our work are based on hyperbolic mirrors. This shape is the solution of quadric surfaces that provides a central perspective projection where one of its two foci is fixed at the pinhole camera,  $\mathbf{F}^{\text{ii}}$  and the other at the viewpoint,  $\mathbf{F}^{\text{i}}$ . The initial restrictions of our omnidirectional system prototype are imposed by the previously acquired high-resolution cameras. The camera model is the Ueye UI-1485LE-C/M, colour RGB, with resolution of  $2560 \times 1920$ , sensor size equals to  $1/2''$ , 6 fps,  $2.2 \mu\text{m}$  pixel pitch.

The geometry of a hyperbolic catadioptric system is described by means of mirror surface ( $\mathbf{M} \in \mathfrak{R}^3$ ), an arbitrary 3D point in the world space  $\mathbf{X}_W$  and the intersected point of the light ray of  $\mathbf{X}_W$  towards  $\mathbf{F}^{\text{i}}$  at the mirror surface  $\mathbf{X}_M$ . Let the Cartesian coordinates' origin is denoted as  $\mathbf{O}_W$ , the distance between two foci as  $c$ , the distance from  $\mathbf{F}^{\text{ii}}$  to the images of plane is designated as the focal length  $f$ , the projection of the refracted ray that passes through it into the image plane ( $\mathbf{I} \in \mathfrak{R}^2$ ) as  $\mathbf{u}_i = (u_i, v_i)$ , the azimuthal radius as  $\mathbf{r}_M = (X, Y)$  (See fig. 3) if  $\mathbf{O}_W$  is placed on the middle of  $c$ , then the equations of the hyperbolic system are expressed by the following relations and its two foci are  $\mathbf{F}^{\text{i}} = (0, 0, c/2)$  and  $\mathbf{F}^{\text{ii}} = (0, 0, -c/2)$ :

$$\frac{\left(Z - \frac{c}{2}\right)^2}{a^2} - \frac{Y^2 + X^2}{b^2} = 1, \quad (1)$$

$$\|\mathbf{r}\| = \sqrt{X^2 + Y^2}. \quad (2)$$

Since the perspective projection is rotationally symmetric about  $\hat{\mathbf{z}}$ -axis, the problem can be restricted to the  $\hat{\mathbf{z}}\hat{\mathbf{r}}$ -plane and the mirror shape as a profile in the 2D plane. The

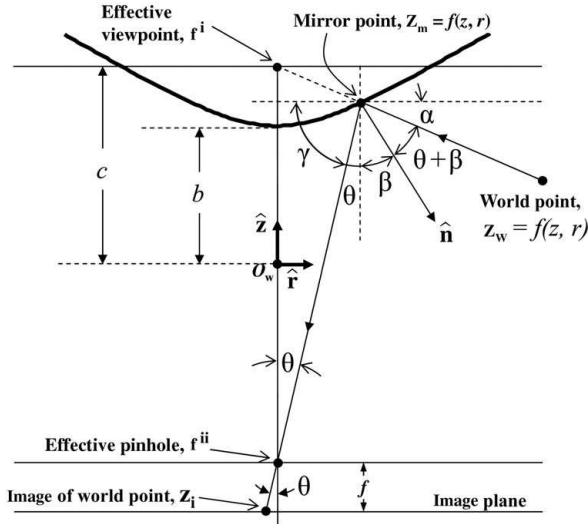


Fig. 3. Hyperbolic catadioptric system geometry.

problem consists in finding an appropriate mirror profile that suits the camera restrictions such as depth of field, working area and, last but not less important, the minimum focus distance. The geometry used to derive the fixed viewpoints as mentioned above has been presented in refs. [17, 18]. As it is well known in the field of perspective cameras' geometry, the relationship between a point in a 3D space ( $\vec{X}_M = [X_M, Y_M, Z_M, 1]^T$ ) and its projection onto the image frame ( $\vec{u}_i = [u_i, v_i, 1]^T$ ), both expressed in homogeneous coordinates, can be associated according to the equation  $\vec{u}_i = \mathbf{K}\mathbf{\Pi}\vec{X}_M$ , where  $\mathbf{K}$  and  $\mathbf{\Pi}$  are the intrinsic and extrinsic camera parameter matrices.

Figure 3 illustrates the hyperbolic catadioptric system geometry in the 2D Cartesian coordinates. As in 3D representation, the two foci are aligned along  $\hat{z}$ -axis, where  $\mathbf{f}^i = (0, c/2)$  and  $\mathbf{f}^{ii} = (0, -c/2)$ . The mirror profile is a function  $z(r)$ , where  $r$  comes from Eq. (2), the arbitrary world point is  $\mathbf{z}_w = (z_w, r_w)$ , the intersection of the incoming light ray at the mirror surface is  $\mathbf{z}_m = (z_m, r_m)$  and finally the point where the refracting light ray intersects the image plane is denoted by  $\mathbf{z}_i = (z_i, r_i)$ . The angle  $\theta$  is the vertical angle of the camera and its complementary angle is  $\gamma$ , and  $\alpha$  is the angle between  $\hat{r}$ -axis and the incoming light ray from  $\mathbf{z}_w$ . Subsequently,  $\beta$  is the angle between  $\hat{z}$ -axis and the normal  $\hat{n}$  to  $\mathbf{z}_m$ , therefore the slope at this point is

$$\frac{dz}{dr} = -\tan \beta. \quad (3)$$

Finally, the vertical angle of the catadioptric system is  $\phi = 2\beta + \theta$ . Next, the following relationships can be deduced:

$$\theta = 90^\circ - \gamma, \quad (4)$$

$$180^\circ = \gamma + 2\theta + 2\beta + \alpha. \quad (5)$$

Substituting Eq. (4) in Eq. (5):

$$2\beta = \gamma - \alpha. \quad (6)$$

Taking the tangent on Eq. (6) and using standard trigonometry relations, such as  $\tan(2\beta)$ ,  $\tan(\gamma - \alpha)$  and the slope (3), the resultant equation is

$$4rz \left( \frac{dz}{dr} \right)^2 - (4r^2 + c^2 - 8z^2) \left( \frac{dz}{dr} \right) - 4rz = 0. \quad (7)$$

The resolution of the catadioptric system must be computed to avoid the degeneration of the geometric relation among the points in a 3D space, the information observed by  $\mathbf{f}^i$ , and its projection in an open disk. This fact is important to obtain correct panoramic and perspective image transformations. The resolution can be defined as the relation between an infinitesimal area on the image  $dP$  and its corresponding solid angle of the world  $d\omega$ ; detailed description of the method was presented by Benosman and Kang in ref. [28]. Due to geometrical properties of the hyperbola it is possible to derive the solution by consecutive relations between  $dP$  and an infinitesimal area on the mirror surface.

Several simulations have been performed to solve the first-order differential Eq. (7) and consequently to find an appropriate profile that suits the camera parameters, the mean dimensions of a human head and the ability of acquiring a wide vertical field of view. We have performed a simulation of the mirror profile and the resulting hyperbolic mirror designed and manufactured (using CNC micro-mechanisation facilities at the Centre for Automation and Robotics – CSIC-UPM) is presented in Fig. 4. The resulting omnidirectional images acquired by the developed system, and the rectified panoramic as well as its cylindrical representation are shown in Fig. 5.

Other solutions for Eq. (7) can be found in refs [29, 30], where restrictions such as a logarithmic sensor or the proposal for constant resolution cameras, are suggested.

#### 4. Catadioptric Panoramic Stereovision System

The stereovision problem for omnidirectional systems is analogous as for conventional cameras are concerned. The epipolar geometry has been studied thoroughly in ref. [19], which describes the relationship of corresponding 3D points between a pair of images by means of epipolar lines that for the case of catadioptric systems are curved. To present the geometry of our proposed omnidirectional stereo system, the initial step is to consider two catadioptric cameras: *1-omnivision* and *2-omnivision* with an already known geometry (i.e. see Fig. 3). In order to simplify the notation, only the variables related to the mirror and world frame will be retained because their projection onto the image plane can be controlled and *vice versa* from the image plane data onto the mirror frame (please refer to Section 3). The catadioptric systems are positioned in such way that their viewpoints are horizontally aligned, their local  $\hat{z}$ -axes are parallel to each other and DH is the distance between them. The catadioptric system is depicted in Fig. 6, where  $\tilde{\mathbf{X}}_W$  is taken as an arbitrary point in the 3D space and its reflecting light rays at both mirrors' surfaces are  $\tilde{\mathbf{X}}_M^1 = (X_M^1, Y_M^1, Z_M^1)$  and  $\tilde{\mathbf{X}}_M^2 = (X_M^2, Y_M^2, Z_M^2)$ , respectively. Depending on sensors geometry ( $c_1 \leq \text{hor}c_1 \geq h$ ),  $c_1$  can take different values.

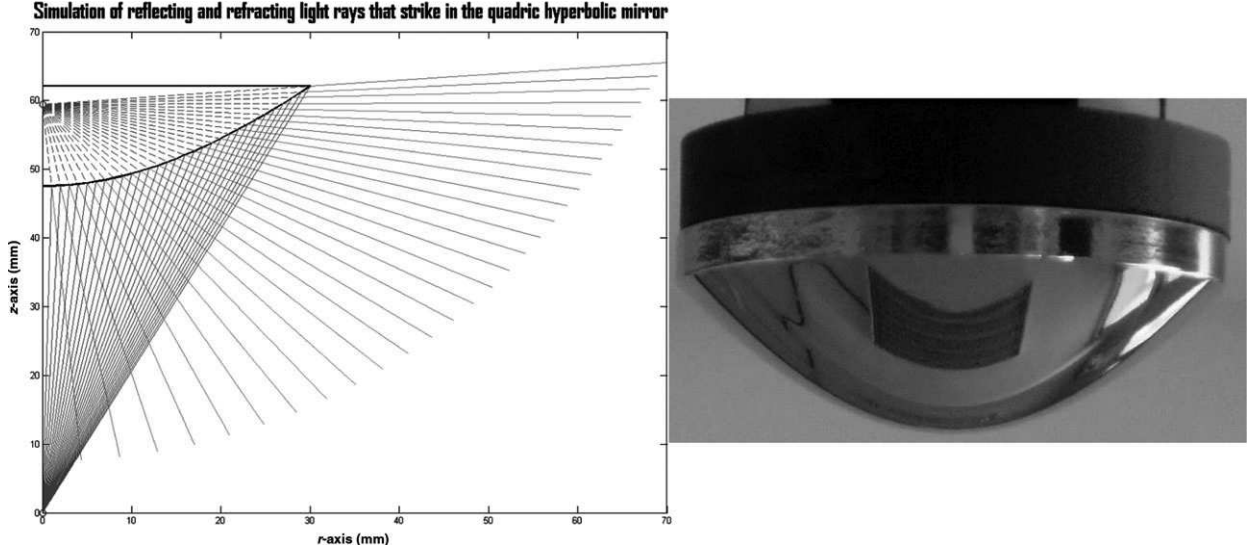


Fig. 4. (Colour online) Hyperbolic mirror. (a) Reflecting ray lights that strike the mirror surface; (b) real image of the specially manufactured mirrors by CNC micro-mechanisation.

Assume that the origin  $\tilde{\mathbf{O}}_W$  of the 3D coordinate system is located at  $\tilde{\mathbf{F}}_2^{\text{ii}}$  (2-omnivision).

Noticing that variables in the world frame  $\tilde{\mathbf{O}}_W$  are like “ $\tilde{\mathbf{A}}$ ,” the coordinates in the local frame  $\mathbf{O}_W$  are transformed to  $\tilde{\mathbf{O}}_W$  by  $\tilde{\mathbf{A}} = \tilde{\mathbf{O}}_W \mathbf{T}_{\mathbf{O}_W} \mathbf{A}$ . The plane conformed by  $\tilde{\mathbf{F}}_1^{\text{i}} \tilde{\mathbf{F}}_2^{\text{i}} \wedge \tilde{\mathbf{F}}_1^{\text{i}} \tilde{\mathbf{X}}_W$  or  $\tilde{\mathbf{F}}_1^{\text{i}} \tilde{\mathbf{F}}_2^{\text{i}} \wedge \tilde{\mathbf{F}}_2^{\text{i}} \tilde{\mathbf{X}}_W \Rightarrow \tilde{\mathbf{n}}_\Pi$  is denoted as  $\Pi$  and its normal is denoted as  $\tilde{\mathbf{n}}_\Pi$ . Fig. 3 illustrates the geometry of the sensors. The positions of the foci are  $\tilde{\mathbf{F}}_1^{\text{i}} = (D_H, 0, h)$ ,  $\tilde{\mathbf{F}}_2^{\text{i}} = (0, 0, h)$ ,  $\tilde{\mathbf{F}}_1^{\text{ii}} = (D_H, 0, h - c_1)$  and  $\tilde{\mathbf{F}}_2^{\text{ii}} = (0, 0, 0)$ . The baseline  $\tilde{\mathbf{F}}_1^{\text{i}} \tilde{\mathbf{F}}_2^{\text{i}}$  is parallel to  $\hat{\mathbf{x}}$ -axis, so equation for  $\Pi$  is derived as follows:

$$\tilde{\mathbf{F}}_1^{\text{i}} \tilde{\mathbf{X}}_M^{\text{i}} \Rightarrow \tilde{\mathbf{X}}_F^{\text{M}} = (X_M^1 - D_H, Y_M^1, Z_M^1 - h), \quad (8)$$

$$\tilde{\mathbf{F}}_2^{\text{i}} \tilde{\mathbf{F}}_1^{\text{i}} \Rightarrow \tilde{\mathbf{B}}_2^1 = (-D_H, 0, 0), \quad (9)$$

$$\tilde{\mathbf{n}}_\Pi = \tilde{\mathbf{X}}_F^{\text{M}} \times \tilde{\mathbf{B}}_2^1 \Rightarrow \Pi : -D_H (Z_M^1 - h) Y + (D_H Y_M^1) Z. \quad (10)$$

Let us suppose a third camera 3-omnivision is introduced, vertically aligned to 2-omnivision (see Fig. 7), their foci belonging to  $\hat{\mathbf{z}}$ -axis and  $D_V$  is the distance between them. The viewpoint of 3-omnivision is  $\tilde{\mathbf{F}}_3^{\text{i}}$ , and the point at the mirror surface coming from  $\tilde{\mathbf{X}}_W$  is  $\tilde{\mathbf{X}}_M^3$ . The geometry between 3–2-omnivision is defined by the baseline  $\tilde{\mathbf{F}}_2^{\text{i}} \tilde{\mathbf{F}}_3^{\text{i}}$ , in this particular case the epipolar curves are radial lines. The plane containing  $\tilde{\mathbf{F}}_2^{\text{i}} \tilde{\mathbf{F}}_3^{\text{i}} \wedge \tilde{\mathbf{F}}_2^{\text{i}} \tilde{\mathbf{X}}_W$  or  $\tilde{\mathbf{F}}_2^{\text{i}} \tilde{\mathbf{F}}_3^{\text{i}} \wedge \tilde{\mathbf{F}}_3^{\text{i}} \tilde{\mathbf{X}}_W \Rightarrow \tilde{\mathbf{n}}_\Omega$  is  $\Omega$ -plane,  $\tilde{\mathbf{F}}_3^{\text{i}} = (0, 0, h + D_V)$  and  $\tilde{\mathbf{F}}_3^{\text{ii}} = (0, 0, h + D_V - c_3)$  are the foci of 3-omnivision and the equation of  $\Omega$ -plane is

$$\tilde{\mathbf{F}}_3^{\text{i}} \tilde{\mathbf{X}}_M^3 \Rightarrow \tilde{\mathbf{X}}_F^{\text{M}_3} = (X_M^3, Y_M^3, Z_M^3 - (h + D_V)), \quad (11)$$

$$\tilde{\mathbf{F}}_3^{\text{i}} \tilde{\mathbf{F}}_2^{\text{i}} \Rightarrow \tilde{\mathbf{B}}_3^2 = (0, 0, -D_V), \quad (12)$$

$$\tilde{\mathbf{n}}_\Omega = \tilde{\mathbf{X}}_F^{\text{M}_3} \times \tilde{\mathbf{B}}_3^2 \Rightarrow \Omega : (-D_V X_M^2) X + (D_V X_M^3) Y = 0. \quad (13)$$

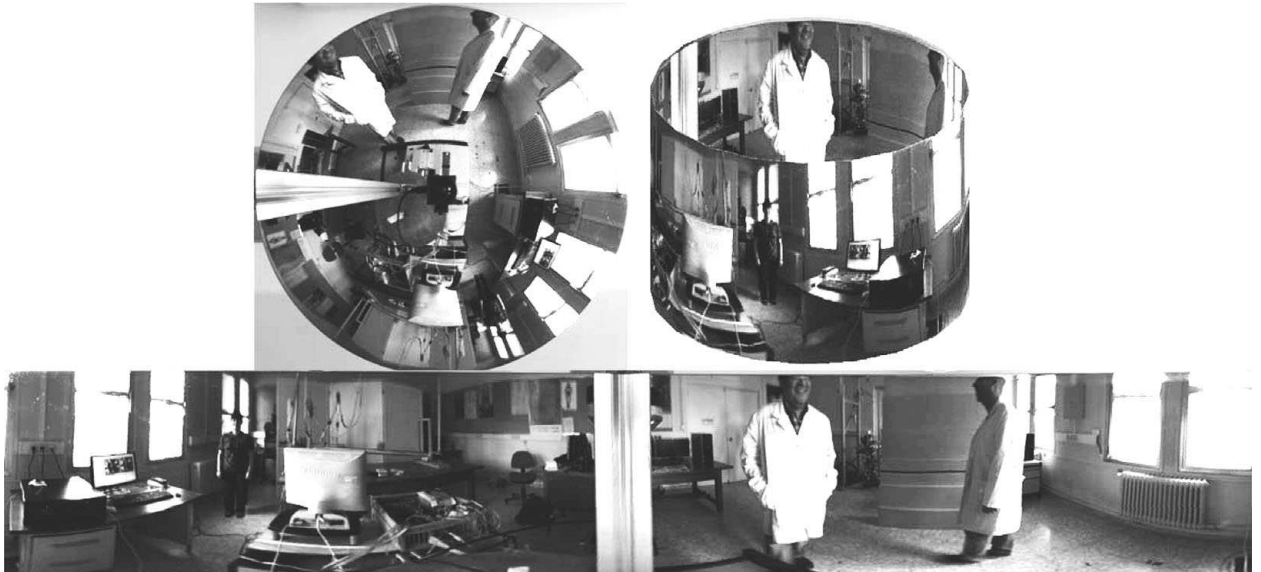


Fig. 5. (Top-left) omnidirectional image; (top-right) cylindrical representation and (bottom) panoramic image.

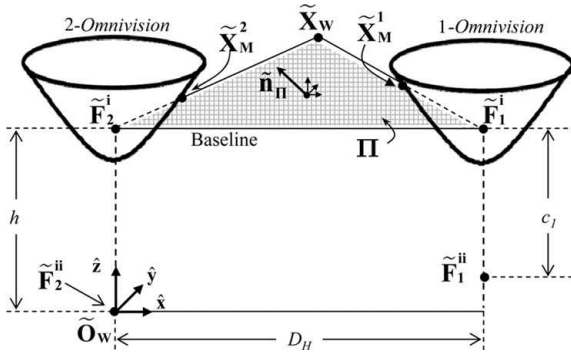


Fig. 6. Stage # 1 for the epipolar geometry of two parallel omnidirectional vision systems with hyperbolic mirrors.

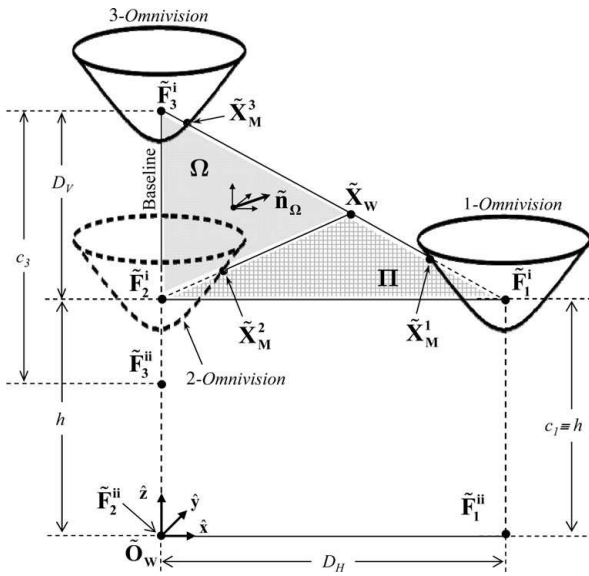


Fig. 7. Complete model for the epipolar geometry of three omnidirectional vision systems, two parallel and one aligned vertically.

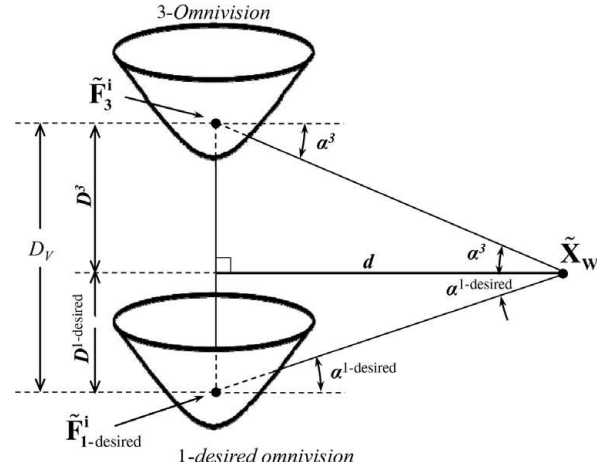


Fig. 8. Triangulation and depth computation of two catadioptric systems aligned vertically.

leading to  $\tilde{X}_M^2 \Rightarrow \tilde{X}_M^{1-\text{desired}}$  (see Fig. 7). If we compute  $\tilde{X}_M^{1-\text{desired}}$ , it will be possible to get a vertically aligned rectified configuration with two decoupled high-resolution catadioptric systems. The theory and properties of rectified images were presented by Hartley in ref. [31]. For catadioptric systems, the rectification process<sup>20,32</sup> provides epipolar radial lines onto the image plane and when they are projected onto the panoramic perspective, they become parallel lines to the vertical axis. Consequently, the depth is isotropic in all directions.

As the points  $\tilde{X}_M^1$  and  $\tilde{X}_M^3$  are known positions, the rectification process becomes a problem for solving the equation system of the intersection between  $\Omega$ -plane (Eq. (13)),  $\Pi$ -plane (Eq. (10)) and the quadric equation of the mirror of 2-omnivision (named  $M_{1-\text{desired}}$ , Eq. (1)). The system has two possible solutions, which are the intersections of the planes ( $\Omega$ - and  $\Pi$ -planes) with the mirror surface  $M_{1-\text{desired}}$ .

However, since the azimuthal angle of the  $\tilde{X}_M^3$  has been computed and it must be same for  $\tilde{X}_M^{1-\text{desired}}$ , it is then possible to select the correct solution for  $\tilde{X}_M^{1-\text{desired}}$ .

Once  $\tilde{X}_M^{1-\text{desired}}$  has been calculated, the problem for depth estimation from a pair of catadioptric systems is reduced to

Table II. Pseudo-code for objects detection and depth estimation.

#### Imaging procedure

1. Image acquisition:
  - Two images (img 1-1 and img 1-2) acquisition by 1-omnivision.
  - Two images (img 3-1 and img 3-2) acquisition by 3-omnivision.
2. Motion detection (segmentation):
  - Image segmentation (imgSeg1): between img 1-1 and img 1-2.
  - Image segmentation (imgSeg3): between img 3-1 and img 3-2.
3. Feature extraction:
  - $F_{\text{omni } 1} = \{\text{motion, colour}\} \Rightarrow \text{ROI}_{\text{omni } 1}$
  - $F_{\text{omni } 3} = \{\text{motion, colour}\} \Rightarrow \text{ROI}_{\text{omni } 3}$
4. Rectification: transformation 1-omnivision to 2-omnivision (1-desired omnivision), Eqs. (13), (10) and (1).
5. Disparity map and depth computation between imgSeg<sub>1-desired</sub> and imgSeg<sub>3</sub> by Eq. (14).
6. Closest object localisation strategies.



472 a simple triangulation, similar to what happens when using  
 473 conventional cameras. Figure 8 illustrates the triangulation  
 474 and depth computation process where  $\alpha_3$  and  $\alpha_{1-\text{desired}}$   
 475 can be obtained from Figs. 3 and 7 and Eqs. (4) and (5), so depth  
 476  $d$  is obtained using the following equation:

$$\left. \begin{aligned} D_V &= D^{1-\text{desired}} + D^3 \\ \tan(\alpha^{1-\text{desired}}) &= \frac{D^{1-\text{desired}}}{d} \\ \tan(\alpha^3) &= \frac{D^3}{d} \end{aligned} \right\} \Rightarrow d$$

$$= \frac{D_H}{\tan(\alpha^{1-\text{desired}}) + \tan(\alpha^3)}. \quad (14)$$

477 It is common that when rectification of images is been  
 478 doing some region onto the image plane will present singu-  
 479 larities or will be occluded in one of the images. Hence, these  
 480 regions must be identified and avoided. In the case of our sys-  
 481 tem, the regions close to two epipoles and the centre of the im-  
 482 ages are where these singularities or occlusions are created.

## 483 5. Experimentation

484 Our goal for the experimental stage is to present an initial  
 485 approach for human-like behaviour by means of the attitude  
 486 of our proposed humanoid head. The visual servoing control  
 487 task is focused in the attention strategies where the system  
 488 reacts to any movements in its surroundings, in this case to  
 489 the nearest moving object.

490 The first stage involves image processing for the  
 491 omnidirectional vision system. Promising results in  
 492 matching correspondences depend on previous segmentation  
 493 procedures. Commonly, robust techniques, such as the well-  
 494 known methods of Mean-shift, CAMshift<sup>33</sup> and so on are  
 495 applied. However, since our purpose is to introduce robots  
 496 in dynamic and changing environments for real-time tasks,  
 497 we have used a robust algorithm for motion segmentation  
 498 based on robust affine regression,<sup>35,36</sup> and also proposed  
 499 in previous work,<sup>34</sup> where several experiments in hard dynamic  
 500 outdoor scenes have been successfully carried out. In order  
 501 to obtain robust feature for interest regions, we also include  
 502 the variance and mean of the colour RGB of each segmented  
 503 region. Then the rectification of the system is applied to the  
 504 segmented regions (solving the equation system of Eqs. (10)  
 505 and (13)) and the disparity map is computed (see Eq. (14)).  
 506 The pseudo code used for this stage is summarised in Table II.

507 In order to present the results of the image procedure, we  
 508 have selected a representative pairs of images from large  
 509 image sequences acquired with the panoramic stereo system  
 510 (top 1-*omnivision* and bottom 3-*omnivision*), displayed in  
 511 Fig. 9. It is possible to observe three interesting situations,  
 512 the first an easiest scenario when a single object is moving in  
 513 the surroundings of the system (see Fig. 9(a)). In the second  
 514 pair, another object enters the scene; therefore, the current  
 515 problem involves multiple moving objects' detection (see  
 516 Fig. 9(b)). The third pair shows several objects that move in  
 517 random trajectories around the system (see Fig. 9(c)). The  
 518 sequences were acquired in dynamic changing scenarios with

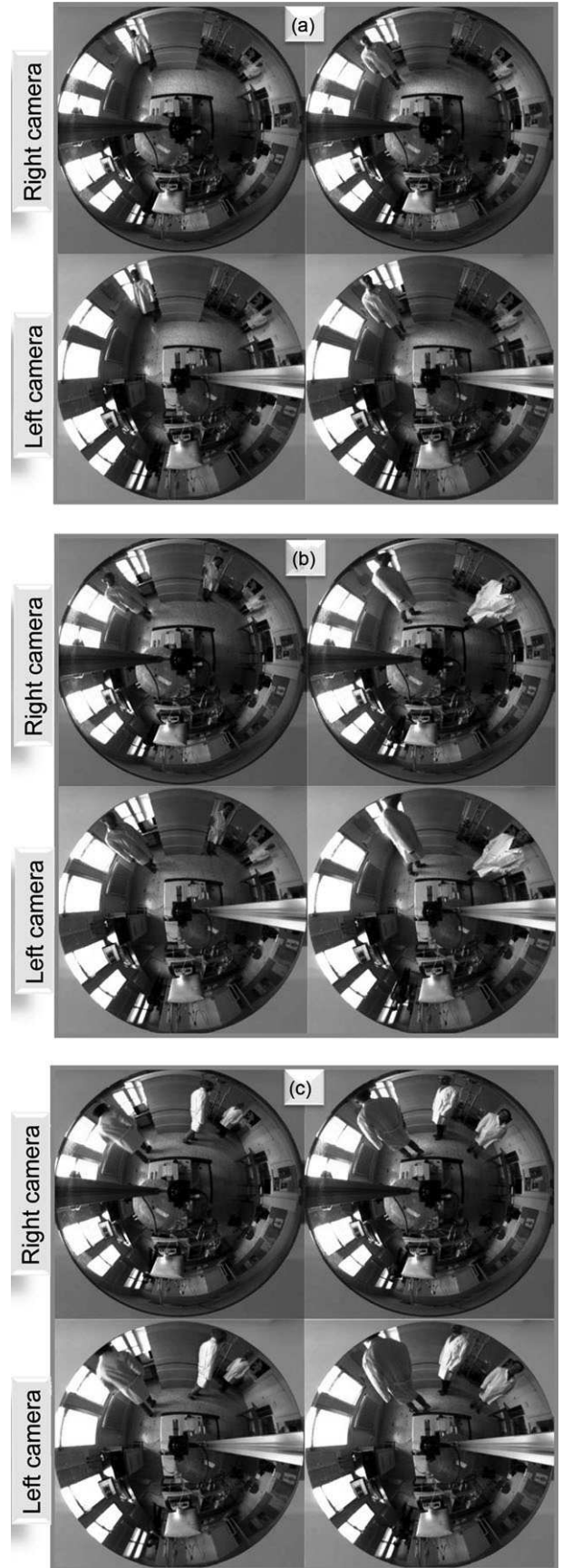


Fig. 9. (Colour online) Omnidirectional images sequences: three pairs from (top) 1-*omnivision* and (bottom) 3-*omnivision*.



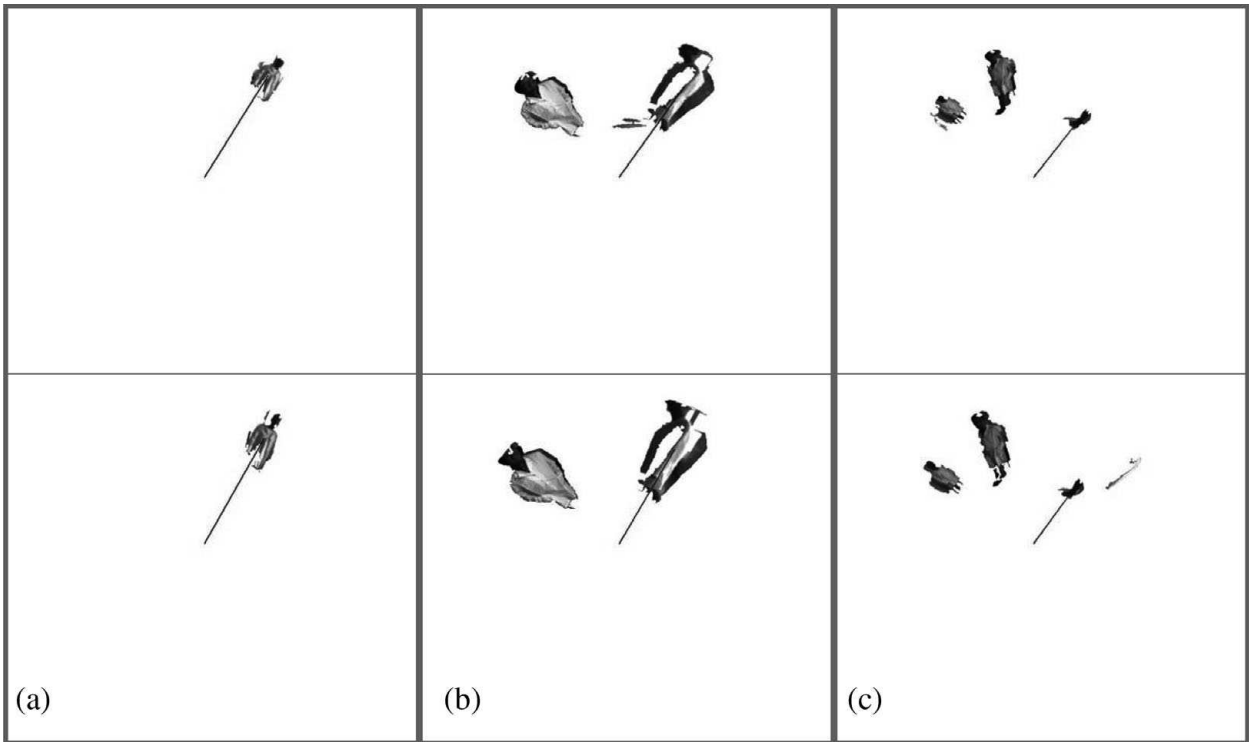


Fig. 10. The robust motion segmentation of image pairs and feature extraction for ROI.

519 uncontrolled light conditions; it is possible to observe the  
 520 light coming through the window.

521 The extraction of robust features of the regions (objects –  
 522 possible targets) in movement is the main goal of the image-  
 523 processing stage (see Table II). The combination of the  
 524 robust algorithm for motion detection and region clustering  
 525 by means of the gradient of colour variances allows us to  
 526 compensate the changes in light conditions. Figure 10 shows  
 527 the motion detection and feature extraction of three pairs of  
 528 images. These three pairs describe similar situations as the  
 529 images presented in Figs. 9(a), (b) and (c), respectively.

530 Q8 Once the regions of interest (ROI) are identified on  
 531 both segmented images, we transform 1-omnivision to 2-  
 532 omnivision (1-desired omnivision). When the images are  
 533 vertically aligned, the disparity can be computed (inversely  
 534 proportional to depth) for each ROI, therefore the nearest  
 535 object can be defined. In order to perform the process of  
 536 matching correspondences, the translation of the ROI needs  
 537 a transformation due to catadioptric resolution. Figure 11  
 538 exemplifies a disparity map and depth representation where  
 539 the darker objects represent the nearest regions of interest.  
 540 In addition, as a result of the disparity calculation, in Fig. 10  
 541 the nearest object of each pair of images, captured by 1-  
 542 omnivision and 3-omnivision, is selected by a radial line  
 543 from the image centre.

544 Several experiments were performed in order to test the  
 545 visual attention control strategy, the results generated for the  
 546 vision system for tracking the nearest object are presented  
 547 as a function of the angular position (the elevation  $\beta$  and the  
 548 azimuthal  $\alpha$  angles), distances (*disp.*) and magnitude of the  
 549 movement ( $\mathbf{M}$ ). The decision stage weighs the disparity and  
 550 magnitude of the movement to select the nearest object; in  
 551 this way the system will let alone near static objects and will

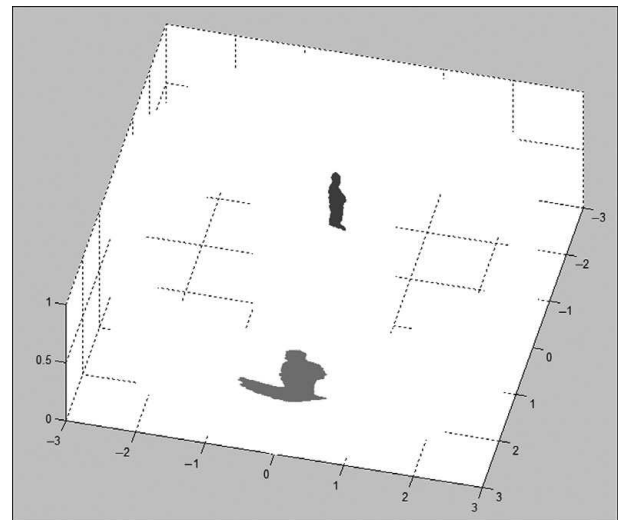


Fig. 11. Disparity map of the objects in motion, dark grey is the closest.

552 attend the next nearest object with the largest movement. 552  
 553 Under this rule our humanoid head will move in a “curious” 553  
 554 human-like manner. 554

555 In Fig. 12 we present the results of the elevation ( $\varphi$ ) and 555  
 556 the azimuthal ( $\alpha$ ) angles, obtained by the omnidirectional 556  
 557 stereovision system – a long and large image sequence, the 557  
 image processing of this initial approach takes  $\sim 300$  ms. Q8

559 Three interesting cases are represented in Fig. 12. In case 1, 559  
 560 the system is tracking the trajectory of an object in movement 560  
 561 (*Object\_1*), and unexpectedly another object moves (*Ob-* 561  
 562 *ject\_2*), a swiftly movement (to kick, to drop something, etc), 562  
 563 since the position of *Object\_2* with respect to the humanoid 563  
 564 head is closer than *Object\_1*, the system attends this action. 564

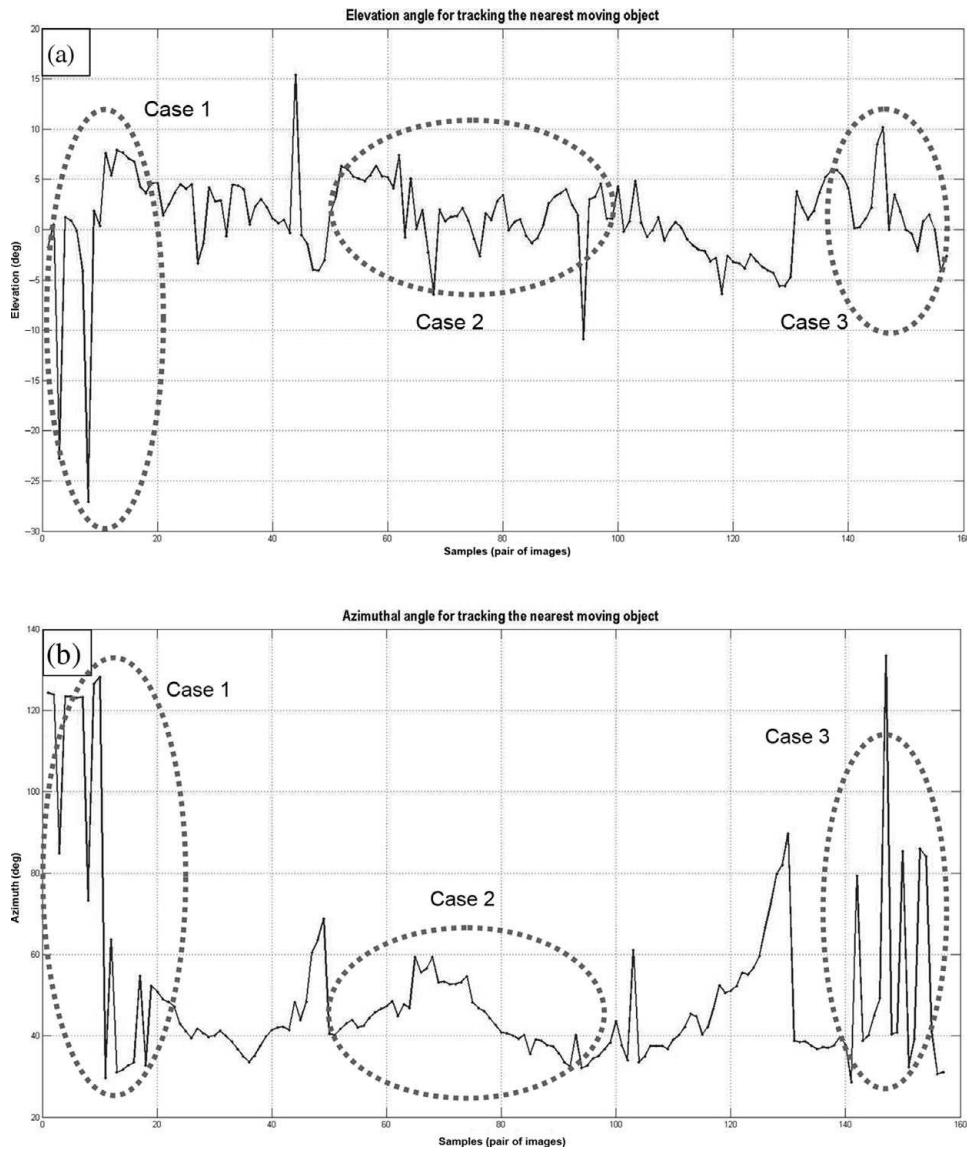


Fig. 12. Experimental results obtained by omnidirectional stereovision system: (a) elevation angle; (b) azimuthal angle.

565 This is represented as outliers in the natural tracking of  
 566 *Object\_1* (this scenario is represented in Fig. 10(c)).

567 The second case (case 2) shows the natural tracking of the  
 568 nearest object in movement (*Object\_1*), where none of the  
 569 objects is nearer than *Object\_1*, this situation is presented

570 in Fig. 10(a). And finally (case 3), a scenario where two  
 571 people are interacting around the human head at equivalent  
 572 distances; in this case both people are selected intermittently  
 573 as a target, for example when people are talking, moving  
 574 their hands and so on (see Fig. 10(b)).

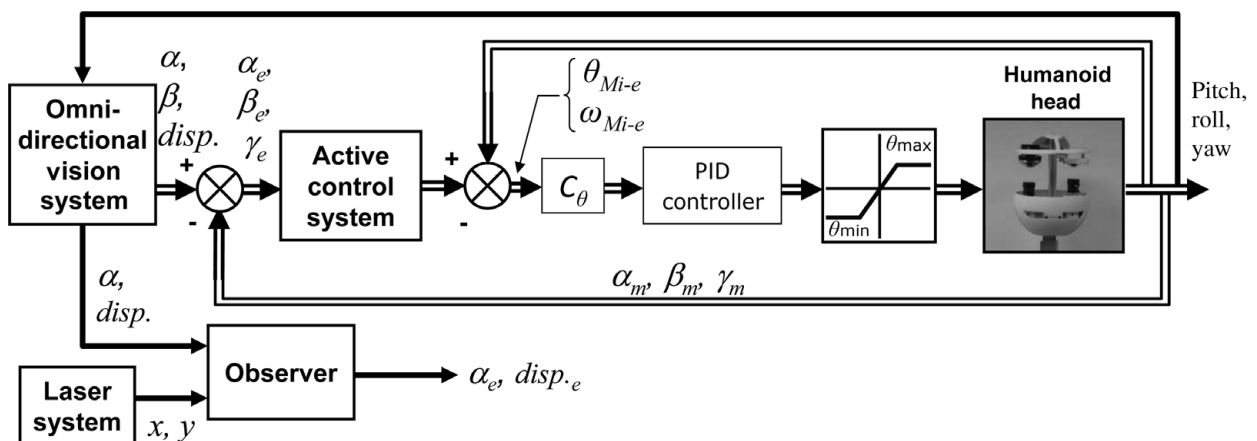


Fig. 13. Block Diagram of active control system for humanoid head using omnidirectional stereovision system.

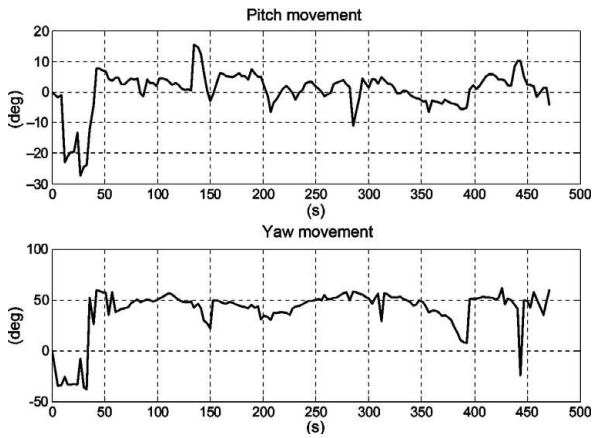


Fig. 14. Experimental results obtained by active control system for tracking the nearest object.

Figure 13 shows a block diagram of the active control system of the humanoid head using omnidirectional stereovision system. The omnidirectional stereovision system supplies the control system input, the azimuth angle ( $\alpha$ ), the elevation angle ( $\beta$ ) and the disparity of the images ( $disp.$ ). Both the azimuth angle and the disparity of the images provided by the omnidirectional stereovision system are validated with data from the laser system, Sick LMS-291,

verifying the effectiveness of the vision system and algorithm described in Table II. Angles  $\alpha$ ,  $\beta$  and  $disp.$  values supplied by the vision system are the inputs for active control system of the humanoid head, so the head can “seek” the objects in movements. The actions carried out by the humanoid head are the pitch ( $\beta$ ), roll ( $disp.$ ,  $\beta$ ) and yaw ( $\alpha$ ). The angular displacements of the neck are limited by the control system to perform natural tracking tasks.

Figure 14 shows the pitch and yaw movements of the humanoid head according to the results presented in Fig. 12. The results of the pitch and yaw movement (Fig. 14) are equivalent to the results of the elevation and azimuthal angles given in Fig. 12. There is a difference between these, because as a normal human behaviour the attention of the humanoid head changes if the most interesting condition appears on scenario. The commands to the active control system are consecutively refreshed when an object is detected by the omnidirectional vision system.

Several experiments were realised in order to test the basic visual servoing control algorithm. In this case (Fig. 15) the omnidirectional stereovision system detects three people in movement, and the vision system is able to localise the closest one. On the other hand, the system can detect the most distant object if it is moving and the nearest objects are in static position. Subsequently, the humanoid head turns its “attention” (central point of the catadioptric system) to the

583  
584  
585  
586  
587  
588  
589  
590  
591  
592  
593  
594  
595  
596  
597  
598  
599  
600  
601  
602  
603  
604  
605  
606  
607  
608



Fig. 15. Experimental testing of the implemented visual servoing algorithm to detect moving objects using omnidirectional stereovision system.

609 central point of the nearest object (or moving object in the  
610 area detected by the vision system).

611 When two or more moving objects interact with each other  
612 at similar distances with respect to the humanoid head, it  
613 performs oscillatory movements paying attention to all them.

614 The behaviour of the humanoid head, briefly described  
615 above, can be noted in the photographic sequences shown  
616 in Fig. 15. Sequences depicted in Fig. 15 should be read  
617 from left to right and top to bottom. In each picture there are  
618 arrows that indicate the attitude of the humanoid head (pitch  
619 and yaw angles) and the area towards the humanoid head  
620 turns his attention.

## 621 6. Conclusions

622 A systematic study of the proposed omnidirectional vision  
623 system was carried out in order to present a reconfigurable  
624 stereovision system for an adaptive humanoid head. The  
625 selected approach consists of panoramic stereovision system,  
626 composed by two hyperbolic catadioptric systems, resulting  
627 finally in a compact high resolution configuration easy to  
628 reproduce and feasible for real-time applications. A specially  
629 designed hyperbolic mirror was also micro-manufactured  
630 in the Centre for Automation and Robotics (CSIC-UPM).  
631 In addition, a simplified method for depth estimation was  
632 presented.

633 Initial experimental results have been introduced. As an  
634 illustration of good performance of the proposed system, a  
635 wide range of typical human-like scenarios was used for these  
636 experiments. We have validated the stereo omnidirectional  
637 vision system (depth estimation) and the target position  
638 (azimuthal angle) by using as reference system such as  
639 LIDAR range sensor.

640 The problem of singularities and lateral occlusions  
641 decreases the range of view; nevertheless this problem  
642 can be solved by using the neck movement. Since the  
643 objects position could be computed and tracked, the system  
644 could gather the situation when an object is approaching to  
645 singularities or occlusions.

## 646 Acknowledgments

647 This research was partially funded by Consejería de  
648 Educación de la Comunidad de Madrid under grant  
649 RoboCity2030 S-2009/DPI-1559, and Agencia Española de  
650 Cooperación Internacional para el Desarrollo (AECID) under  
651 grant FORTUNA D/030531/10. Dr. H. Montes acknowledges  
652 the support received from Universidad Tecnológica de  
653 Panamá and CSIC under JAE-Doc Programme.

## 654 References

- 655 1. Y. Sakagami, R. Watanabe, C. Aoyama, S. Matsunaga,  
656 N. Higaki and K. Fujimura, "The Intelligent ASIMO:  
657 System Overview and Integration," *In: Proceedings of the*  
658 *IEEE/RSJ, International Conference on Intelligent Robots and*  
659 *Systems*, EPFL, Lausanne, Switzerland (Sep. 30–Oct. 4, 2002)  
660 pp. 2478–2483.
- 661 2. K. Kaneko, F. Kanehiro, S. Kajita, H. Hirukawa, T. Kawasaki,  
662 M. Hirata, K. Akachi and T. Isozumi, "Humanoid Robot HRP-  
663 2," *In: Proceedings of the IEEE International Conference on*

- Robotics and Automation*, New Orleans, LA (Apr. 26–May 1, 664  
2004) pp. 1083–1090. 665
3. F. Tanaka and H. Suzuki, "Dance Interaction with QRIO:  
666 A Case Study for Nonboring Interaction by Using an  
667 Entrainment Ensemble Model," *In: Proceedings of the 13th*  
668 *IEEE International Workshop on Robot and Human Interactive*  
669 *Communication*, ROMAN (Sep. 20–22, 2004) pp. 419–  
670 424. 671
4. S. Lohmeier, K. Loffler, M. Gienger, H. Ulbrich and F. Pfeiffer,  
672 "Computer System and Control of Biped 'Johnnie'," *In:*  
673 *Proceedings of the IEEE International Conference on Robotics*  
674 *and Automation*, New Orleans, LA, Vol. 4 (Apr. 26–May 1,  
675 2004) pp. 4222–4227. 676
5. C. L. Breazeal, Sociable Machines: Expressive Social  
677 Exchange between Humans and Robots *Ph.D. Dissertation*  
678 (Massachusetts Institute of Technology, Cambridge, MA,  
679 USA, 2000). 680
6. R. Brooks, C. Breazeal, M. Marjanović, B. Scassellati and M.  
681 Williamson, *The Cog Project: Building a Humanoid Robot*,  
682 *Lecture Notes in Computer Science (LNCS)*. (Springer-Verlag,  
683 Heidelberg, Germany, 1999) pp. 52–87. 684
7. J. Hirth, N. Schmitz and K. Berns, "Emotional Architecture for  
685 the Humanoid Robot Head ROMAN," *In: Proceedings of the*  
686 *IEEE International Conference on Robotics and Automation*,  
687 Roma, Italy (Apr. 10–14, 2007) pp. 2150–2155. 688
8. E. Yoshida, J-P. Laumond, C. Esteves, O. Kanoun, A. Mallet,  
689 T. Sakaguchi and K. Yokoi, "Motion autonomy for humanoids:  
690 experiments on HRP-2 No. 14," *Comput. Animat. Virtual*  
691 *Worlds* **20**, 511–522 (2009). 692
9. O. Stasse, B. Verrelst, B. Vanderborght and K. Yokoi,  
693 "Strategies for humanoid robots to dynamically walk over large  
694 obstacles," *IEEE Trans. Robot.* **25**(4), 960–967 (2009). 695
10. J. Chestnutt, P. Michel, J. Kuffner and T. Kanade,  
696 "Locomotion Among Dynamic Obstacles for the Honda  
697 ASIMO," *Proceedings of the 2007 IEEE/RSJ International*  
698 *Conference on Intelligent Robots and Systems*, San Diego, CA,  
699 USA (Oct 29–Nov 2, 2009). 700
11. F. Pfeiffer, "The TUM walking machines," *Phil. Trans. R. Soc.*  
701 **365**(1850), 109–131 (2007). 702
12. D. W. Rees, "Panoramic Television Viewing System," US  
703 Patent No. 3505465 (1970). 704
13. J. Hong, "Image Based Homing," *In: Proceedings of*  
705 *the International Conference on Robotics and Automation*,  
706 Sacramento, USA (1991) pp. 620–625. 707
14. K. Yamazawa, Y. Yagi, M. Yachida, "Omnidirectional Imaging  
708 with Hyperboloidal Projection," *In: Proceedings of the*  
709 *IEEE/RSJ International Conference on Intelligent Robots and*  
710 *Systems*, Yokohama, Japan (Jul. 26–30, 1993) pp. 1029–  
711 1034. 712
15. Y. Yagi, Y. Nishizawa and M. Yachida, "Map-based navigation  
713 for a mobile robot with omnidirectional image sensor COPIS,"  
714 *IEEE Trans. Robot. Autom.* **11**(5), 634–648 (1995). 715
16. C. Geyer and K. Daniilidis, "Catadioptric projective geometry,"  
716 *Int. J. Comput. Vision* **45**(3), 223–243 (2001). 717
17. T. Svodoba, "Central Panoramic Cameras Design, Geometry,  
718 Egomotion," *Ph.D. Thesis* (Center for Machine Perception,  
719 Czech Technical University, Prague, Czech Republic, 1999). 720
18. S. Baker and S. K. Nayar, "A theory of single-viewpoint  
721 catadioptric image formation," *Int. J. Comput. Vis.* **35**(2), 1–22  
722 (1999). 723
19. T. Svodoba, T. Padjdla and V. Hlavac, "Epipolar Geometry  
724 for Panoramic Cameras," *In: Proceedings of the European*  
725 *Conference on Computer Vision*, Bombay, India (Jan. 1998)  
726 pp. 218–232. 727
20. J. Gluckman, S. K. Nayar and K. J. Thoresz, "Real-Time  
728 Omnidirectional and Panoramic Stereo," *In: Proceedings of*  
729 *DARPA Image Understanding Workshop* (Nov. 1998) pp. 299–  
730 303. 731
21. E. L. Cabral, J. C., Junior and M.C. Hunold, "Omnidirectional  
732 Stereo Vision with a Hyperbolic Double Lobed Mirror,"  
733 *Proceedings of the Pattern Recognition, 17th International*  
734 *Conference*, Vol. 1 (IEEE CS Press, Washington, DC, 2004). 735

- 736 22. S. A. Nene and S. K. Nayar, "Stereo with Mirrors," **In:** 762  
737 *Proceedings of International Conference on Computer Vision,* 763  
738 Bombay, India (Jan. 1998) pp. 1087–1094. 764
- 739 23. M. Armada, R. Caballero, T. Akinfiyev, H. Montes, C. Manzano, 765  
740 L. Pedraza and P. González de Santos, "Design of SILO2 766  
741 Humanoid Robot," **In:** *Proceedings of IARP Workshop on* 767  
742 *Humanoid and Friendly Robotics*, Tsukuba, Japan (Dec. 11– 768  
743 12, 2002) pp. 37–42. 769
- 744 24. H. Montes, "Análisis, diseño y evaluación de estrategias de 770  
745 control de fuerza en robots caminantes," *Ph.D. Thesis* (U. 771  
746 Complutense, Spain, 2005). 772
- 747 25. H. Montes, C. Salinas, G. Fernandez, P. Clarembaux, P. 773  
748 Gonzalez de Santos and M. Armada, "Omnidirectional 774  
749 Stereo Vision Head for Humand Robots," **In:** *Proceedings* 775  
750 *of CLAWAR'09*, Istabul, Turkey (Sep. 9–11, 2009) pp. 909– 776  
751 918. 777
- 752 26. D. A. Winter, *Biomechanics and Motor Control of Human* 778  
753 *Movement* (John Wiley, Hoboken, NJ, 1990). 779
- 754 27. A. Vasavada, L. Siping and S. Delp, "Influence of muscle 780  
755 morphometry and moment arms on the moment-generating 781  
756 capacity of human neck muscles," *SPINE* **23**(4), 412–422 782  
757 (1998). 783
- 758 28. R. Benosman and S. B. Kang, *Panoramic Vision: Theory* 784  
759 *System and Applications* (Springer-Verlag, New York, 785  
760 2001). 786
- 761 29. T. Padjdla, "Localization Using SVAVISCAs Panoramic Image 787  
of Agam Fiducials – Limits of Performance," *Technical Report* 788  
(Center for Machine Perception, Czech Technical University, 762  
Prague, Czech, 2001). 763
30. J. Gaspar, C. Deccó, J. Okamoto and J. Santos-Victor, 764  
"Constast Resolution Omnidirectional Cameras," *Proceedings* 765  
*of Workshop on Omni-Directional Vision*, Copenhagen, 766  
Denmark (2002). 767
31. R. Hartley and A. Zisserman, *Multiple View Geometry in* 768  
*Computer Vision* (Cambridge University Press, Cambridge, 769  
UK, 2004). 770
32. Z. Zhu, "Omnidirectional Stereo Vision," *Workshop on* 771  
*Omnidirectional Vision, Proceedings of the 10th IEEE ICAR,* 772  
Budapest, Hungary (2001). 773
33. D. Comaniciu and P. Meer. "Mean shift: A robust approach 774  
toward feature space analysis," *IEEE Trans. Pattern Anal.* 775  
*Mach. Intell.* **24**(5), 603–619 (2002). 776
34. C. Salinas and M. Armada, "Analysing Human-Robot 777  
Interaction Using Omnidirectional Vision and Structure from 778  
Motion," *Proceedings of CLAWAR'08*, Coimbra, Portugal 779  
(2008). 780
35. M. Black, "The robust estimation of multiple motions: 781  
Parametric and piecewise smooth flow fields," *Comput. Vis.* 782  
*Image Underst.* **63**(1), 75–104 (1996). 783
36. A. Bab-Hadiashar and D. Suter, "Robust optical flow 784  
computation," *IJCV* **29**(1), 59–77 (1998). 785
37. E. R. Davies, *Machine Vision, Third Edition: Theory, ~~Q13~~* 786  
*Algorithms, Practicalities (Signal Processing and its* 787  
*Applications)* (Morgan Kaufmann, Massachusetts, 2005). 788